Fuel 323 (2022) 124407

Contents lists available at ScienceDirect

Fuel

journal homepage: www.elsevier.com/locate/fuel

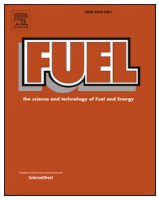

Full Length Article

PAH formation characteristics in hydrogen-enriched non-premixed hydrocarbon flames

Chinonso Ezenwajiaku *, Midhat Talibi, Ramanarayanan Balachandran

Department of Mechanical Engineering, University College London, London WC1E 7JE, UK

ARTICLE INFO

Keywords:
PAH
Planar laser induced fluorescence
Hydrogen
Methane
Soot
Laminar inverse diffusion flame

ABSTRACT

The utilisation of hydrogen with conventional hydrocarbons offers an excellent opportunity to decarbonise current energy systems without significant hardware upgrades. However, this presents fresh scientific challenges, one of which is the difficulty in effective control of pollutant soot emissions due to complex reaction kinetics of hydrogen enriched flames. This paper focuses on polycyclic aromatic hydrocarbons (PAHs), which are the building blocks of soot and responsible for its carcinogenicity. Detailed understanding of the effect of H_2 on the underlying processes of PAH formation and growth is important for the development of effective strategies to curtail PAH formation and hence, reduce soot emissions from combustion systems.

In this study, an experimental methodology was employed to analyse PAH formation and growth characteristics of laminar inverse diffusion flames of various hydrocarbon fuels (alkanes and alkenes) enriched with H_2 using simultaneous planar laser induced fluorescence (PLIF) imaging of PAHs and hydroxyl radicals (OH). OH PLIF was used to indicate peak temperature locations in the flame (flame front), while PAH PLIF was used to determine PAH formation characteristics. Methane (CH_4) was also separately added to the same hydrocarbon fuels to study effects of carbon-bound hydrogen addition, in comparison to H_2 addition. It was observed that only the addition of H_2 to CH_4 showed significant variation in the magnitude of PAH reduction levels as the length along the flame front, L_f increased. The results also showed that while the addition of H_2 was more effective in reducing the rate of PAH fluorescence signal increase (indicative of concentration growth) when compared to CH_4 addition, both fuels showed two distinct regions in the PAH growth curve; a steep growth region followed by a slower growth region. This is potentially indicative of the self-limiting nature of PAH formation and growth. The study concluded that the growth rate of PAHs lies within a narrow band irrespective of the fuel bonding, molecular structure and the H:C ratio of the fuel mixtures tested.

1. Introduction

Air pollution due to prevalent hydrocarbon combustion remains of great concern due to its adverse effect on human health and the environment. Soot particles are known to be toxic to humans potentially leading to cardiovascular and respiratory complications [1,2]. Soot emissions can also have serious implications for the environment, contributing to climate change [3]. Polycyclic aromatic hydrocarbons (PAHs) have been established as dominant precursors (building blocks) of soot particles [4-6]. Therefore, to reduce emissions of soot into the atmosphere, a better understanding of the complex physical and chemical pathways that lead to PAH formation and growth, and eventually to soot production, is necessary. This will not only aid in the improvement of soot formation models, but also inform operation strategies for combustion systems that minimise soot emissions.

Several strategies including the addition of secondary gases and diluents to hydrocarbon fuels have been employed by researchers to investigate reduction in the concentration of PAH and soot, and in addition improve understanding of pathways that lead to their formation and growth. Zhang *et al.* [7] studied the effects of adding CO_2 and water vapour on PAH formation in laminar premixed ethylene-oxygen-argon flame using laser induced fluorescence (LIF) and kinetic simulation. They observed a monotonic decrease in PAH LIF intensity as the addition of both CO_2 and water vapour increased, with water vapour showing better effectiveness in PAH reduction than CO_2. The authors reported that the addition of CO_2 increased the backward reaction rate of $CO + OH \rightleftharpoons CO_2 + H$ decreasing the concentration of H radical and increasing the OH radical concentration. Similarly, the addition of water

* Corresponding author.
E-mail address: chinonso.ezenwajiaku@ucl.ac.uk (C. Ezenwajiaku).

https://doi.org/10.1016/j.fuel.2022.124407
Received 3 February 2022; Received in revised form 2 April 2022; Accepted 24 April 2022
Available online 4 May 2022

vapour increased the backward reaction rate of OH + OH ⇌ O + H_2O and CH_3 + OH ⇌ CH_2* + H_2O resulting in increased formation of OH radical. The authors attributed the reduction in PAHs to this increase in OH radical (through enhanced oxidation rates) and depletion of H radical (reduced H abstraction rate). McEnally and Pfefferle [8] studied the effect of adding N_2 to laminar non-premixed CH_4 and ethylene flames on PAH formation. The authors utilised mass spectrometry techniques and reported a reduction in maximum centreline PAH concentration with increase in N_2 volume flow rate which was attributed to the dilution effect caused by the non-reacting N_2.

Researchers have also studied the effects of adding H_2 to hydrocarbon fuels on PAH formation and growth. H_2 is of interest because it is considered a zero-carbon energy carrier and has shown potential for the improvement of combustion properties and reduction of pollutant emissions when blended with hydrocarbon fuels for combustion [9]. In their numerical study of H_2-C_2H_4-Air diffusion flames, Guo et al. [10] reported a reduction in PAH growth rate with addition of up to 24% H_2 (*v/v*). This reduction was attributed to the higher concentration of H_2 molecule closer to the burner lip and lower H-atom concentration in the surface growth regions which lowers the abstraction rate of PAHs. They also observed that for a given H_2 addition, the combined effect of high temperature, higher concentration of benzene (first aromatic ring) and acetylene enhanced PAH growth rate as the height above the burner (HAB) increased resulting in higher concentration of pyrene at higher heights. Liu *et al.* [11] studied the effect of adding H_2 to the fuel stream of CH_4 diffusion flames on PAH formation through numerical modelling. They observed a reduction in the mole fraction of PAHs (both benzene and pyrene) with the addition of 30% by volume of H_2 for all the HAB considered. Du et al. [12] investigated the effects of adding various additives including H_2 to counterflow diffusion flames of C_2H_4, C_3H_8 and n-C_4H_{10} on soot formation. They used the local velocity gradient to determine the characteristic soot inception rate (relevant to PAH growth) and laser line extinction measurement for soot volume fractions (SVF). Their results showed that although H_2 addition increased the flame temperature consistently, the sooting inception limits and SVF reduced for all conditions. They attributed this effect to the following reasons: (a) the preferential diffusion of H_2 in strained CDF possibly reduced the concentration of soot precursors (PAH) thereby reducing the soot formation rate, (b) H_2 addition reduces the carbon supply of the main fuel and (c) increased concentration of H_2 in the mixture reverses the H-abstraction reaction of the HACA mechanism ($A_i + H \leftrightarrow A_i^- + H_2$) thus limiting the involvement of the aromatic radical in further mass addition reactions and consequently, reducing the concentration of PAHs available for further growth to soot. Hong-Quan *et al.* [13] studied the effect of adding H_2 in laminar premixed CH_4 flame on nucleation and soot growth process using jet-cooled laser induced fluorescence (LIF), gas chromatography and laser induced incandescence (LII). Their results showed that while the addition of H_2 promotes PAH and soot formation, substitution of some of the CH_4 with H_2 impedes the formation of PAH and soot. The authors also reported that H_2 addition significantly modifies the dynamics of the soot growth process (including coagulation/coalescence processes).

Most conventional fuels and natural gases utilised in practical combustion systems are complex fuel mixtures [14,15]. The individual components in these mixtures play an important role in determining the sooting tendency (soot volume fraction, soot particle size and PAHs) of these practical fuels [16]. As a result, some studies have represented these fuels by mixing carbon/non-carbon fuels to understand the effects of fuel composition on the formation of PAHs and soot [17-21]. Additionally, these studies have shown that chemical interactions between various molecules in binary/ternary mixtures reveal kinetic pathways which provide insight to some complex processes of PAH and soot formation mechanisms which are elusive with single component fuel investigations [16]. Park *et al.* [17] studied the effects of fuel composition on PAH and soot formation in counterflow diffusion flames of gasoline surrogates using LIF, laser induced incandescence (LII) and chemical kinetic modelling. Their work focused on binary mixtures of *n*-heptane/*iso*-octane, *n*-heptane/toluene, *iso*-octane/toluene and ternary mixtures of *n*-heptane/*iso*-octane/toluene. For the binary mixtures with toluene, the authors observed a distinctive synergistic effect on PAH formation with increasing toluene ratio. Synergistic effect refers to the case where the PAH concentration formed from the combustion of the binary fuel mixture is higher than that of the pure fuel. The authors explained that benzyl radicals formed from the dehydrogenation of toluene were key to the synergistic effect on PAH concentration observed. This synergistic effect due to binary mixtures has been observed in other works [18,19,22-24]. Roesler *et al.* [19] investigated binary mixtures of CH_4 and *n*-Heptane in premixed flames, and CH_4/C_2H_4 mixtures in co-flow diffusion flames and flow reactor. They obtained detailed PAH speciation with gas chromatography (GC) coupled with flame ionisation detector (FID) and mass spectrometry (MS) while soot volume fraction was achieved with LII. The authors observed that the addition of CH_4 in C_2H_4 increased the formation of PAH and soot in the reactor and co-flow diffusion flame while no increase was seen for the premixed flame of CH_4/*n*-heptane. Methyl radicals from CH_4 were implicated as responsible for the synergistic effect on PAH in binary mixtures of CH_4/C_2H_4 in the diffusion flame and reactor, which the authors claimed enhanced PAH formation and growth from the propargyl recombination reaction (odd-carbon numbered species). Similar role of methyl radical in the enhancement of PAH formation was reported by Yoon *et al.* [23,24] as the reason for the synergistic effect on PAH and soot formation observed in their study of the binary mixtures of C_2H_4 with C_2H_6, dimethyl ether (DME) and C_3H_8 independently in the counter flow diffusion flame configuration. Liu *et al.* [25] investigated the effect of DME addition to C_2H_4 diffusion flame on PAH and soot formation using PLIF and LII respectively. They also observed a synergistic effect on PAH and soot as the volume of DME in the binary mixture increased and attributed it to increase in methyl radical concentrations produced from the dissociation of DME which enhanced the formation of PAH.

Several open flame configurations have been used for PAH and soot studies in literature. Broadly, this includes the premixed flame and non-premixed flames [7,26,27]. Although both flame configurations can provide important details on the complex processes leading to PAH formation, the non-premixed configuration have been observed to be more suitable to understand the effect of fuel type and in tracking the early stages of PAH formation and growth [28]. There are two common types of non-premixed flames utilised for PAH studies, the normal diffusion flames (NDF) and the inverse diffusion flame (IDF). In the NDF configuration, the fuel is fed through the central tube of the burner surrounded by the oxidiser in an annular ring, while this configuration is reversed to obtain the IDF configuration. For PAH growth studies, the IDF configuration is preferred because in the NDF configuration, the combustion products are convected through the main reaction zones of the flame where they get significantly oxidised and carbonised while the structure of the IDF provides an excellent separation between the pyrolysis and oxidation processes [29,30]. This is because the combustion products are formed on the fuel-rich side of the flame and hence, do not undergo significant oxidisation and carbonisation. It has also been shown to be more relevant to real world combustion applications [30,31].

The above review of literature shows that PAH formation and growth as an important step to soot formation and growth still needs more study for a complete understanding of the process, as various studies have shown contrasting or indefinite conclusions. Also, further insights are required on the growth of PAH to ascertain the relationship between the availability of PAH concentration and how much it grows and perhaps provide experimental evidence for the self-limiting behaviour of PAH and PAH dimerisation. Although the effect of H_2 addition on PAH formation in CH_4 flames is well researched, there is limited information on the effect of H_2 addition on PAH formation in other conventional hydrocarbon fuels, especially in the IDF configuration. This is important as these additional data sets would help provide more insights on the

effects of fuel type (or molecular structure effects) on PAH formation and would help generalise the outcomes for other relevant industrial processes. Therefore, the primary aim of this study is to understand the dependence of PAH growth rate on both PAH LIF signal (as a marker of PAH concentration) and the H:C ratios of different base hydrocarbon fuels through a parametric study. The H:C ratios have been modified to achieve a sufficiently wide range through the addition of either H_2 or CH_4 to allow determination of reliable correlations. The H:C ratio is used to remove the specificity of the fuel component and have a parameter which makes it easy for the PAH growth rate results (or expression) to be benchmarked or extended to any other hydrocarbon mixture(s). Hence, the objectives of the current study are: (1) to investigate the effects of adding H_2 and CH_4 to C1-C3 fuels (CH_4, C_2H_6, C_2H_4, C_3H_8, and C_3H_6) respectively on PAH formation characteristics, (2) estimate the growth rate of PAH concentration in these mixtures and show how it is affected by H_2 and CH_4 addition, (3) determine the relationship between the estimated growth rate and PAH concentration for all mixtures studied and (4) understand differences between the addition of hydrogen through either H_2 or CH_4.

2. Experimental methodology

2.1. Burner description

Fig. 1 shows the schematic of the burner used to stabilise the inverse diffusion flame (IDF) configurations utilised in this study. The inverse diffusion flame provides good separation between the pyrolysis and oxidative process in the flames and as a result, produces relatively unaltered larger amount of PAH and soot. The burner has been previously described in [30,32], therefore, a brief summary is presented here. The burner consists of three coaxial stainless-steel tubes with inside diameters of 10, 30 and 64 mm for the central, annular inner and outer co-flow passages respectively. In the IDF configuration, the air and fuel mixture flow through the central and inner co-flow tubes respectively. To minimise air entrainment effects from the ambient, nitrogen was passed through the outer co-flow passage. All three tubes had a knife-edge finish at the exit of the burner to minimise effects of rim thickness. A combination of steel balls (of diameters 3 mm and 5 mm), wire mesh and honeycomb ensured flow smoothing and straightening.

2.2. Simultaneous OH and PAH LIF imaging

The schematic for the laser and camera setup for the simultaneous measurement of OH radicals and PAH LIF signal is shown in Fig. 2. The laser system for this study consists of a combination of an Nd:YAG Laser (Litron Nano-PIV) and a tunable dye laser (Fine Adjustments Pulsare-S model) with Rhodamine 6G dye. For the excitation of the OH radical, a frequency-doubled output from the Nd:YAG Laser was used to pump the tunable dye laser. The output from the dye laser was frequency-doubled and tuned to near 283 nm to obtain the Q1(5) transition of the $A^2\Sigma^+ \leftarrow X^2\Pi(1,0)$ band with approximately 160 mJ/cm^2 laser fluence. A right-angle prism, plano-concave cylindrical lens (f = -40 mm) and bi-convex lens (f = 500 mm) were used to convert the beam to a light sheet with height of 50 mm, which was aligned with the central axis of the burner.

PAH excitation was also achieved with the same laser sheet described above to allow for simultaneous OH-PAH measurement. It was noted from literature that PAH LIF emissions are insensitive to excitation wavelength in the range between 265 and 297 nm [33]. There is ample literature demonstrating interference from soot particles on PAH LIF measurement in diffusion flames as a result of resonant radiation from laser induced incandescence [34-37]. To prevent this, the laser fluence level was kept to 160 mJ/cm^2(as mentioned earlier). This is similar to the strategy used in [24,34] to avoid noise from soot incandescence.

Two intensified charge coupled devices (ICCDs) cameras placed perpendicular to the direction of the laser sheet on either side of the burner (Fig. 2) were utilised in capturing the OH and PAH LIF signal simultaneously. ICCD-1 (see Fig. 2) fitted with a UV 100 mm f/2.8 Cerco lens and a combination of UG11 and WG305 Schott glass filters was used for the detection of OH fluorescence near 310 nm.

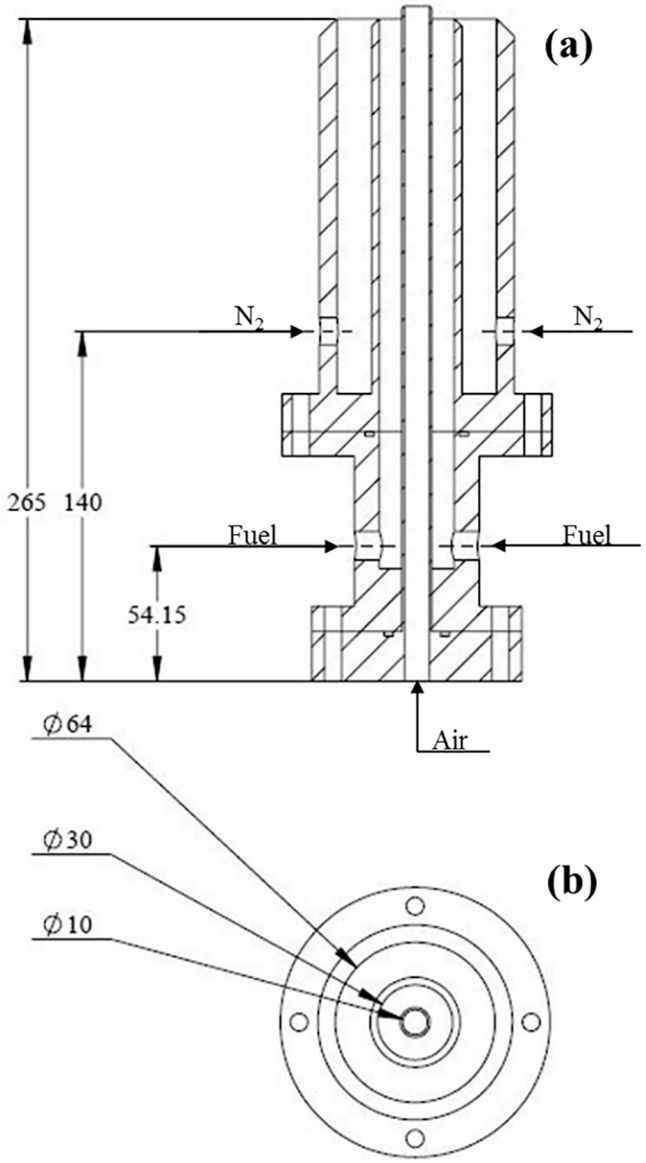

Fig. 1. (a) Side and (b) top view cross sections of the inverse diffusion flame burner showing the diameters of the central and annular passages for the air, nitrogen and fuel. All dimensions are in mm.

For the PAH species, the fluorescence was captured on ICCD-2 (see Fig. 2) using a f/1.2 Nikon lens of focal length 50 mm. A combination of GG420 (high pass Schott filter) and BG12 (low pass Schott filter) was fitted to the lens to image fluorescence from PAH species in the wavelength range of 420 nm and 480 nm. This range has been shown to be representative of PAH species of three or more rings [38,39]. Reasons for the choice of PAH detection regime and suitability of the LIF technique for PAH analysis have been discussed in details in our previous study [40].

2.3. Flow conditions and control

PAH formation characteristics of the binary mixtures of each of the five primary fuel gases – methane/CH_4, ethane/C_2H_6, propane/C_3H_8, ethylene/C_2H_4, and propylene/C_3H_6 - with hydrogen/H_2 and CH_4 were

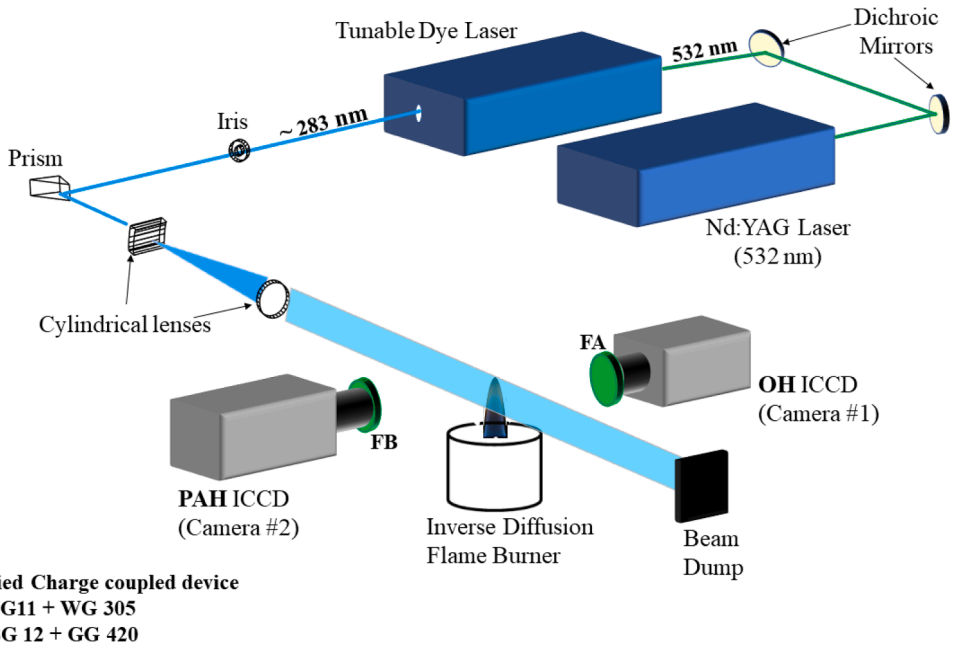

Fig. 2. Schematic of the experimental arrangement used for simultaneous planar laser induced fluorescence imaging of PAH and OH.

investigated. The number of carbon atoms was kept constant (=12) for the base case of each primary fuel gas to enable comparison between them. Hence, the flowrate of the respective primary gases (before the addition of H_2 or CH_4) was 12 slpm, 6 slpm and 4 slpm for C_1 (CH_4), C_2 (C_2H_6 & C_2H_4) and C_3 (C_3H_8 & C_3H_6) fuels respectively. Thermal mass flow meters (Vögtlin Instruments and Bronkhorst flow meters) fitted with high precision needle valves were used for independent control and metering of all gas flows (air, CH_4, C_2H_6, C_2H_4, C_3H_8, C_3H_6, H_2 and nitrogen/N_2) to the burner. The accuracy of all the flow meters was ± 1.5% full scale division (FSD). Table 1 below shows details of the flow conditions for the fuel mixtures investigated in this study.

Two sets of experiments were conducted. In the first set, H_2 was added to each of the primary fuels in varying percentages (up to 17% for CH_4, 33% for C_2H_6 and C_2H_4, 50% for C_3H_8 and C_3H_6). This was to compare the effect of H_2 addition on PAH formation in these fuels and create well resolved range of H:C ratio for the comparison between PAH LIF signal (representative of concentration) and growth rate to be described later. In the second set, CH_4 was added to the primary fuels in varying percentages (up to 50% for C_3H_6, 60% for C_3H_8 and 80% for C_2H_6 and C_2H_4). These sets of CH_4 addition experiments were conducted to understand the differences between the addition of molecular hydrogen (H_2) and addition of carbon-bound hydrogen (through the addition of CH_4) and also create a good range for the H:C ratio comparison as described for the H_2 addition case. Overall, the data could help establish if there is any significant correlation between PAH growth and PAH LIF signal based on H:C ratio in this study.

For each primary fuel set investigated, the exit velocity was kept constant by reducing the primary fuel flow rate as the flow rate of the secondary fuel was increased.

2.4. Growth rate of PAH LIF

An important aspect of PAH study is the role it plays in the formation of soot particles. PAHs grow from smaller rings to larger rings (as well as increase in concentration) as the height (above burner exit) increases in a flame. These larger ring PAHs subsequently aggregate to form soot. Hence, determining the rate of this growth and the role an increase in PAH concentration plays downstream of the flame is key to understanding the transition to soot formation. The relationship between the PAH growth rate and the PAH concentration can be regarded as the self-assembly characteristics of PAH. This growth process can be assumed to occur via the HACA mechanism as proposed by Frenklach [41] and dimerisation of PAHs [42,43].

The growth rate characteristics of PAH for most practical combustion experiments are presented as a function of the height above burner (HAB). This captures the growth characteristics in terms of distance (residence time and velocity). Alternatively, modelling approaches (0D or 1D) for the growth of PAH are in terms of concentration as a function of time. However, this approach does not capture the height effects (spatial resolution). In this study, we attempt to transform the HAB-derived PAH data into concentration growth characteristics for PAH since PAH growth in flames is a pyrolytic process which depends on the local PAH availability, and the obtained PAH LIF signal is primarily dependent on the number density of the PAH species as observed in our previous study [40]. Here, the growth characteristics refer to the rate of change of PAH LIF signal with respect to distance along the flame front, L_f (which is representative of HAB). This PAH growth is assumed to be a consequence of increase in both PAH concentration and the number (or size) of rings formed as L_f increases. For this study, growth rate of PAH concentration is determined from the established PAH LIF curves. The PAH LIF curves are smoothened with a polynomial fit of second order (chosen because it showed the best fit to the data in this study) and then differentiated in segments of 0.5 mm along the length of the curve using the central difference method to achieve the first derivative ($d(PAH)/dL_f$) of each segment. The obtained derivative gives the growth rate of PAH LIF signal in this study; where $d(PAH)$ refer to the change in the PAH LIF signal and dL_f is the change in distance along the flame front.

2.5. Image processing and analysis

Fig. 3 shows the averaged and combined PAH and OH LIF images with illustrations of the parameters used for the analysis in this study. For each test condition, 200 instantaneous images each of OH and PAH are captured and averaged to obtain a single representative image for PAH and OH respectively. Due to the difference in resolution between PAH and OH images, the averaged OH image is warped with sub-pixel accuracy onto the PAH image using an in-house developed image warping MATLAB® code to obtain Fig. 3(a).

A detailed explanation of the image analysis employed in this study

Table 1
Summary of the flow conditions for the fuel mixtures investigated. fp – Primary fuel; fs – secondary fuel; Q_{fp} – volume flow rate of primary fuel, Q_{fs} – volume flow rate of secondary fuel; Q_{air} – volume flow rate of air (fixed at 1.2 slpm), T_{ad} – adiabatic temperature; Re – Reynolds number (fuel).

fp – CH_4, fs – H_2, Q_{air} – 1.2 slpm					
Q_{fp} (slpm)	Q_{fs} (slpm)	Q_{fs} (%)	H:C	T_{ad}	Re
12.0	0.0	0	4.00	2226.0	445.5
11.6	0.4	3	4.07	2231.1	440.0
11.2	0.8	7	4.14	2237.8	434.6
10.8	1.2	10	4.22	2242.8	429.4
10.4	1.6	13	4.31	2247.7	426.8
10.0	2.0	17	4.40	2254.3	419.3
fp – C_2H_6, fs – H_2, Q_{air} – 1.2 slpm					
Q_{fp} (slpm)	Q_{fs} (slpm)	Q_{fs} (%)	H:C	T_{ad}	Re
6.0	0.0	0	3.00	2260.4	234.5
5.6	0.4	7	3.07	2269.3	228.5
5.2	0.8	13	3.15	2276.8	222.8
4.8	1.2	20	3.25	2285.6	217.3
4.4	1.6	27	3.36	2294.3	210.9
4.0	2.0	33	3.50	2301.7	207.2
fp – C_3H_8, fs – H_2, Q_{air} – 1.2 slpm					
Q_{fp} (slpm)	Q_{fs} (slpm)	Q_{fs} (%)	H:C	T_{ad}	Re
4.0	0.0	0	2.67	2267.3	160.5
3.6	0.4	10	2.74	2279.2	153.3
3.2	0.8	20	2.83	2290.9	147.6
2.8	1.2	30	2.95	2302.5	141.4
2.4	1.6	40	3.11	2314.1	135.8
2.0	2.0	50	3.33	2325.6	131.3
fp – C_2H_4, fs – H_2, Q_{air} – 1.2 slpm					
Q_{fp} (slpm)	Q_{fs} (slpm)	Q_{fs} (%)	H:C	T_{ad}	Re
6.0	0.0	0	2.00	2370.1	234.5
5.6	0.4	7	2.07	2370.3	227.0
5.2	0.8	13	2.15	2370.6	222.8
4.8	1.2	20	2.25	2371.1	216.0
4.4	1.6	27	2.36	2371.7	210.9
4.0	2.0	33	2.50	2372.2	206.0
fp – C_3H_6, fs – H_2, Q_{air} – 1.2 slpm					
Q_{fp} (slpm)	Q_{fs} (slpm)	Q_{fs} (%)	H:C	T_{ad}	Re
4.0	0.0	0	2.00	2335.0	160.5
3.6	0.4	10	2.07	2339.1	154.3
3.2	0.8	20	2.17	2343.4	147.6
2.8	1.2	30	2.29	2347.9	142.3
2.4	1.6	40	2.44	2352.4	136.6
2.0	2.0	50	2.67	2357.1	131.3
fp – C_2H_6, fs – CH_4, Q_{air} – 1.2 slpm					
Q_{fp} (slpm)	Q_{fs} (slpm)	Q_{fs} (%)	H:C	T_{ad}	Re
6.0	0.0	0	3.00	2260.4	234.5
4.8	1.2	20	3.11	2253.6	232.9
3.6	2.4	40	3.25	2246.7	229.9
3.3	2.7	45	3.29	2245.0	228.5
3.0	3.0	50	3.33	2243.3	228.5
2.7	3.3	55	3.38	2241.6	228.5
2.4	3.6	60	3.43	2239.9	227.0
1.8	4.2	70	3.54	2236.4	225.6
1.2	4.8	80	3.67	2232.9	224.2
fp – C_3H_8, fs – CH_4, Q_{air} – 1.2 slpm					
Q_{fp} (slpm)	Q_{fs} (slpm)	Q_{fs} (%)	H:C	T_{ad}	Re
4.0	0.0	0	2.67	2267.3	160.5
2.8	1.2	30	2.83	2255.0	156.3
2.4	1.6	40	2.91	2250.9	155.3
2.2	1.8	45	2.95	2248.9	154.3
2.0	2.0	50	3.00	2246.8	154.3
1.6	2.4	60	3.11	2242.7	152.3
fp – C_2H_4, fs – CH_4, Q_{air} – 1.2 slpm					
Q_{fp} (slpm)	Q_{fs} (slpm)	Q_{fs} (%)	H:C	T_{ad}	Re
‘6.0	0.0	0	2.00	2370.1	234.5
4.8	1.2	20	2.22	2342.9	231.4
3.6	2.4	40	2.50	2314.9	228.5
2.4	3.6	60	2.86	2286.2	227.0
2.2	5.1	70	3.08	2271.4	274.4
2.2	8.8	80	3.33	2256.5	410.9
fp – C_3H_6, fs – CH_4, Q_{air} – 1.2 slpm					
Q_{fp} (slpm)	Q_{fs} (slpm)	Q_{fs} (%)	H:C	T_{ad}	Re
4.0	0.0	0	2.00	2335.0	160.5
2.8	1.2	30	2.25	2303.4	157.4
2.4	1.6	40	2.36	2292.7	155.3
2.2	1.8	45	2.43	2287.3	155.3
2.0	2.0	50	2.50	2281.9	154.3

has been published previously [40] and only a brief description is presented. In diffusion flames, it has been shown that peak temperature region coincides with peak OH concentration [44]. Hence, in this study the reference flame location (flame front) was represented by the loci of the peak of the OH LIF profile. The length along the flame front denoted as L_f is representative of the height above burner (HAB) but with reference to the conical shape of the flame front. This is to allow meaningful comparison between the results of this work and other modelling studies and capture the residence time effects.

An initial starting height above the burner lip, y_o was chosen for all test conditions as the reference point for the length along the flame front, L_f. This starting height (y_o = 1.85 mm for this study) was kept constant across all the test conditions. The PAH profile was determined for the distance, x_n, along a normal axis, n, referenced to the flame front as the origin and extending outwards into the PAH region as shown in Fig. 3a. The resulting profile for this step is shown in Fig. 3b. The same process is repeated for every pixel location on L_f. Each determined PAH profile is cumulated and compared with the corresponding increase in L_f to obtain the PAH formation characteristics for each condition studied. The distance between the position of the maximum PAH LIF signal and the flame front (maximum OH LIF signal) for each x_n is referred as the inter-peak distance (x_{pk}). For each x_n, the profile widths of the PAH and OH are determined at full-width half maximums (FWHMs) and denoted as w_{PAH} and w_{OH} respectively. This method of analysis ensured that the PAHs analysed were subjected to the same temperature–time history and thus, capturing the temperature and the residence time effects in the PAH formation/growth behaviour presented later.

2.6. Uncertainty analysis

To verify the repeatability of the methodology used for this study, the reference case experiment (with no H_2 or CH_4 addition) was performed several times on different days, and the variability in the PAH LIF signals (PAH) was determined to be less than 1%. Prior to expansion of the beam, the central portion of the beam was filtered to remove non-uniformity of the beam edges. As described in our previous study [40], the PAH LIF signal was observed to be independent of the laser intensity beyond 8 mJ (107 mJ/cm^2) of laser energy. Considering the laser shot-to-shot energy variations observed to be within ±10%, a laser fluence of 160 mJ/cm^2 was chosen for this study. This ensured that at the chosen fluence level, the observed variations in the laser fluence (that is 160 ± 16 mJ/cm^2) are still above the threshold value (107 mJ/cm^2) for PAH fluorescence saturation. Hence, it can be concluded that the differences in PAH LIF reported in this study are independent of the laser energy fluctuations.

The accuracy of all the flow meters was ± 1.5% full scale division (FSD). In addition to this value, the set volume flow rate varied by 0.2% for all the conditions tested. The uncertainty due to data smoothening for the determination of the growth rate of PAH LIF signal was estimated to be within ± 3.5% based on the highest standard deviation obtained for all cases.

3. Results and discussion

3.1. Effect of H_2 addition on PAH formation.

Fig. 5 shows normalised PAH LIF signal for the five primary hydrocarbon fuels – C_2H_6, C_2H_4, C_3H_8, C_3H_6 and CH_4 expressed as a function

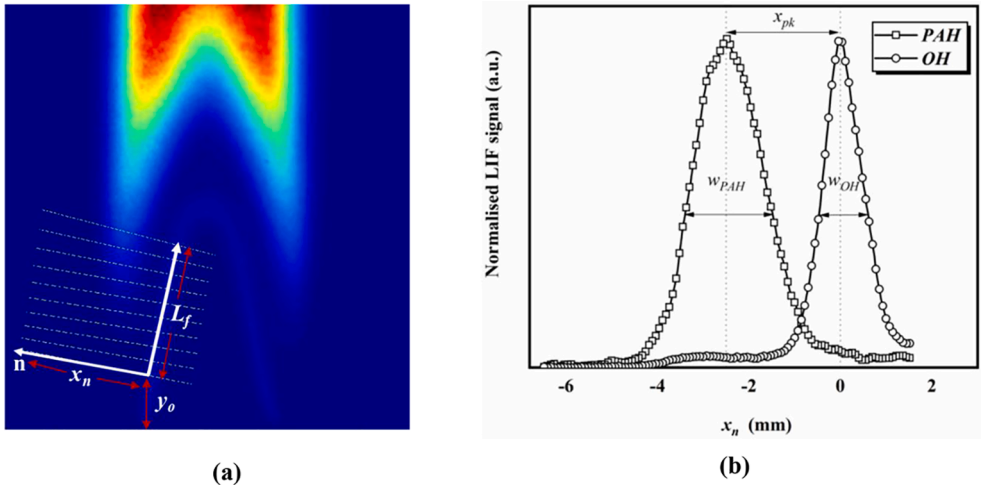

Fig. 3. (a) Shows PAH and OH combined LIF image showing the coordinate systems under consideration with y_o as the initial starting height and normal axis, n (b) PAH and OH line profiles shown here were determined along the distance x_n on the normal axis 'n' referenced to the flame front (L_f).

of percent H_2 addition (v/v) for three different heights along the flame front, L_f. For each L_f, the PAH LIF signal for various percent H_2 addition were normalised with the maximum PAH LIF signal. It can be observed in the cases of C_2H_4, C_3H_8 and C_3H_6 (Fig. 5b, 5c and 5d) that there is no significant variation in magnitude of the reduction levels in PAHs with the addition of H_2 as the L_f increases. This could be attributed to the following; since formation of first ring is an important step to the growth of PAHs and subsequent soot formation [2,28,45], it can be deduced that for C_2H_4, C_3H_8 and C_3H_6, the formation of the first ring and subsequent growth to larger multiple ringed PAHs occur at a very fast rate at lower heights and also could have potentially reached a level where the growth of PAHs saturates such that further growth at higher heights is not observed. These two effects shroud the impact of H_2 addition on PAH growth in these fuels as the height increases. It is reasonable to assume that at lower heights, the rate of PAH growth is fast since it is still in the early phase of the growth process but probably achieves the saturation stage of growth quicker in these fuels because of the higher PAH concentration available and efficiency of the growth process. However, in the CH_4 case, as can be seen from Fig. 5e, addition of H_2 to CH_4 showed higher reductions at higher heights, for example a 17% H_2 addition in CH_4, resulted in a 76% and 44% reduction in PAH LIF signal for 6 mm and 4 mm heights respectively. This is consistent with observations in a previous study by the authors [40] and was attributed to the effectiveness of H_2 in impeding the growth of smaller ring PAHs closer to the burner lip. This limits the concentration of smaller ring PAHs available for growth to larger ring PAHs at higher heights above the burner lip. It is possible in the CH_4 case that though the efficiency of PAH growth is high, it does not have enough PAH concentration available to achieve the saturation stage. This implies that most of the growth process would be in the early phase where the growth process is fast hence the addition of H_2 is expected to be very effective. It is clear from Fig. 5 that with increase in the propensity to form PAH from hydrocarbon fuel studied (that is, as you increase from CH_4 to C_3H_6), the magnitude of reduction in PAH levels as height increase becomes less significant.

Addition of H_2 to CH_4 in this study was limited to 17%, as above that level PAH LIF signal dropped very low leading to very high uncertainty in PAH measurements. Hence, further on comparison between the effect of H_2 additions on the primary fuels will focus on H_2 addition levels of below 17%. Comparing PAH LIF signal at 14% H_2 addition (Fig. 5), shows that the order of PAH reduction from high to low is $CH_4 > C_2H_6 > C_2H_4 > C_3H_8 > C_3H_6$. This order is as expected due to the increasing carbon content and presence of double bonds except for propane showing lower reduction (~30%) than ethylene (~48%) with H_2 addition even though the absolute peak PAH LIF signal in ethylene (*3520 a.u.*) is more than twice that of propane (*1380 a.u.*). According to Frenklach [46], the [H]/[H_2] ratio (ratio of hydrogen atom concentration to molecular hydrogen concentration) is the controlling parameter for the growth of PAH up to the formation of the first soot nuclei. This exception highlighted above could be due to the reason proposed by Gülder et al [47] for the differences they observed with the influence of hydrogen addition in diffusion flames of alkanes and alkenes in their study. They explained that in C_2H_4 pyrolysis, the production of [H_2] and [H] is minimal compared to the concentration produced in C_3H_8 pyrolysis, hence the addition of H_2 in C_2H_4 can be assumed to influence the [H]/[H_2] ratio significantly reducing the rate of PAH production while there might be enough [H] and [H_2] formed from C_3H_8 pyrolysis thereby reducing (shrouding) the effects of added H_2 on PAH reduction in C_3H_8.

3.2. *Effect of CH_4 addition on PAH formation.*

Fig. 6 presents normalised values of PAH LIF signal as a function of percentage CH_4 addition for three different heights along the flame front, L_f. Each test condition was normalised with its respective base case value (that is, primary fuel with no CH_4 addition). A monotonic decrease in PAH LIF signal with CH_4 addition is seen for all the fuels tested (Fig. 6b-d) except for C_2H_6 (Fig. 6a). With C_2H_6, an initial increase in PAH LIF signal is observed with CH_4 addition up to ca. 55% which then sharply reduced afterwards. It is pertinent to note also, that the PAH LIF signal at all heights in the C_2H_6-CH_4 binary mixture prior to 70% CH_4 addition was higher than the base case value. This is due to the synergistic effect between CH_4 and C_2H_6 which results in the corresponding PAH LIF signal of the binary mixture to be higher than those of each individual components in the mixture [23,48]. This synergistic effect will be further discussed later.

It can also be observed from Fig. 6 that the highest reduction in PAH LIF signal occurs at the lowest L_f of 2 mm for all the fuels. For example, with 40% CH_4 addition, a 30% reduction in PAH LIF signal was seen at $L_f = 2$ mm, while a 16% reduction was seen at 6 mm. Similar trend was observed for all the fuels tested. The reason for this observation could potentially be deduced from observations in two studies. Senkan and Castaldi [49] observed two important effects in their study of PAH formation in CH_4 combustion; firstly, first ring formation in the CH_4 flame increased rapidly as the height increases along the reaction zone and secondly the rate of growth from larger ring PAHs to soot was reduced which resulted in a rich pool of PAHs in the gas phase upstream of the flame. In another study, Hepp *et al.* [50] observed some larger PAHs appearing before smaller ones which they attributed to smaller PAHs reacting efficiently by coagulation mechanism to form larger PAHs

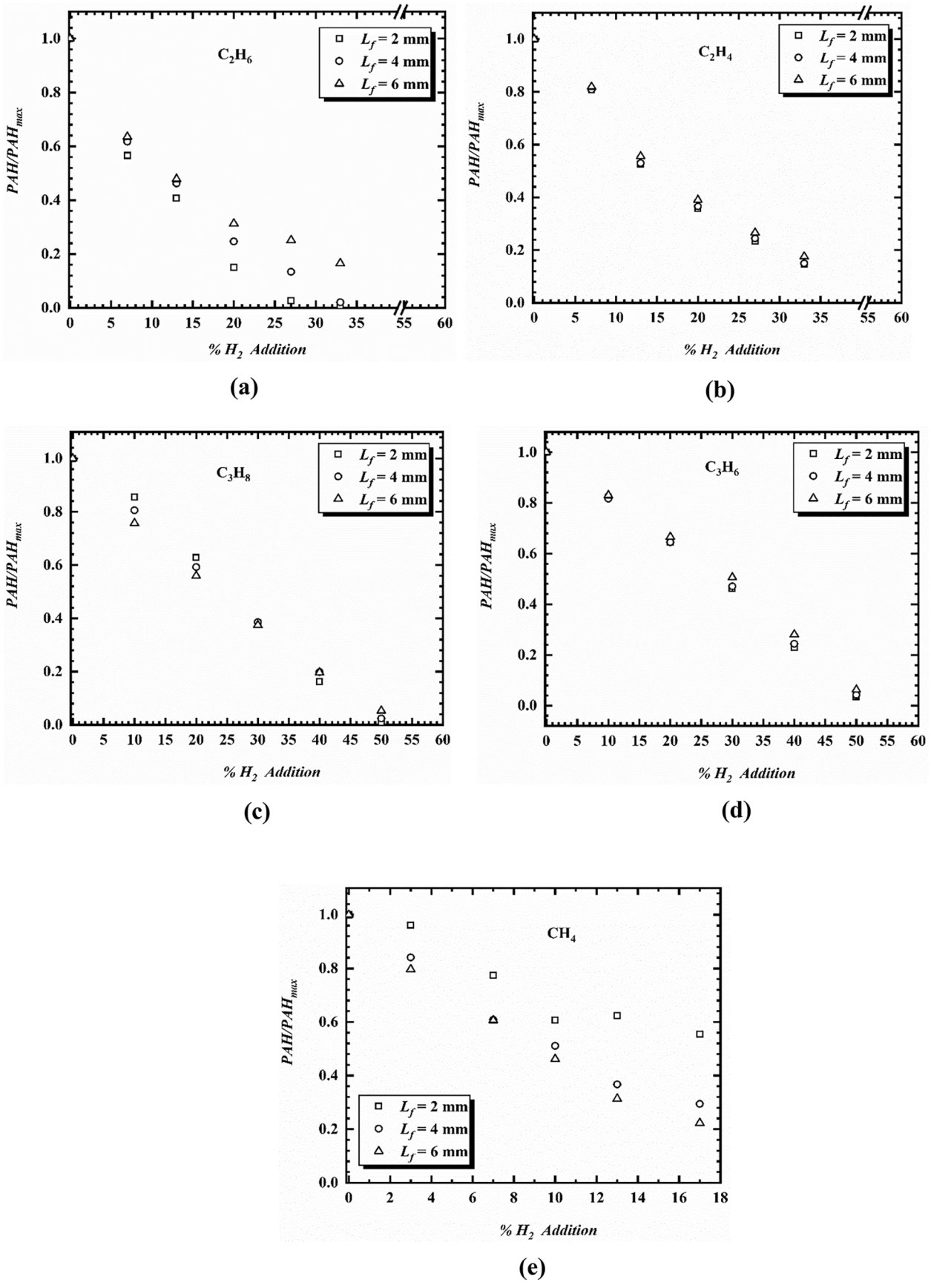

Fig. 5. Variation in the PAH LIF signal normalised using base case value presented as a function of percentage H_2 addition (*v/v*) at three different HAB for (a) C_2H_6 (b) C_2H_4 (c) C_3H_8 (d) C_3H_6 and (e) CH_4.

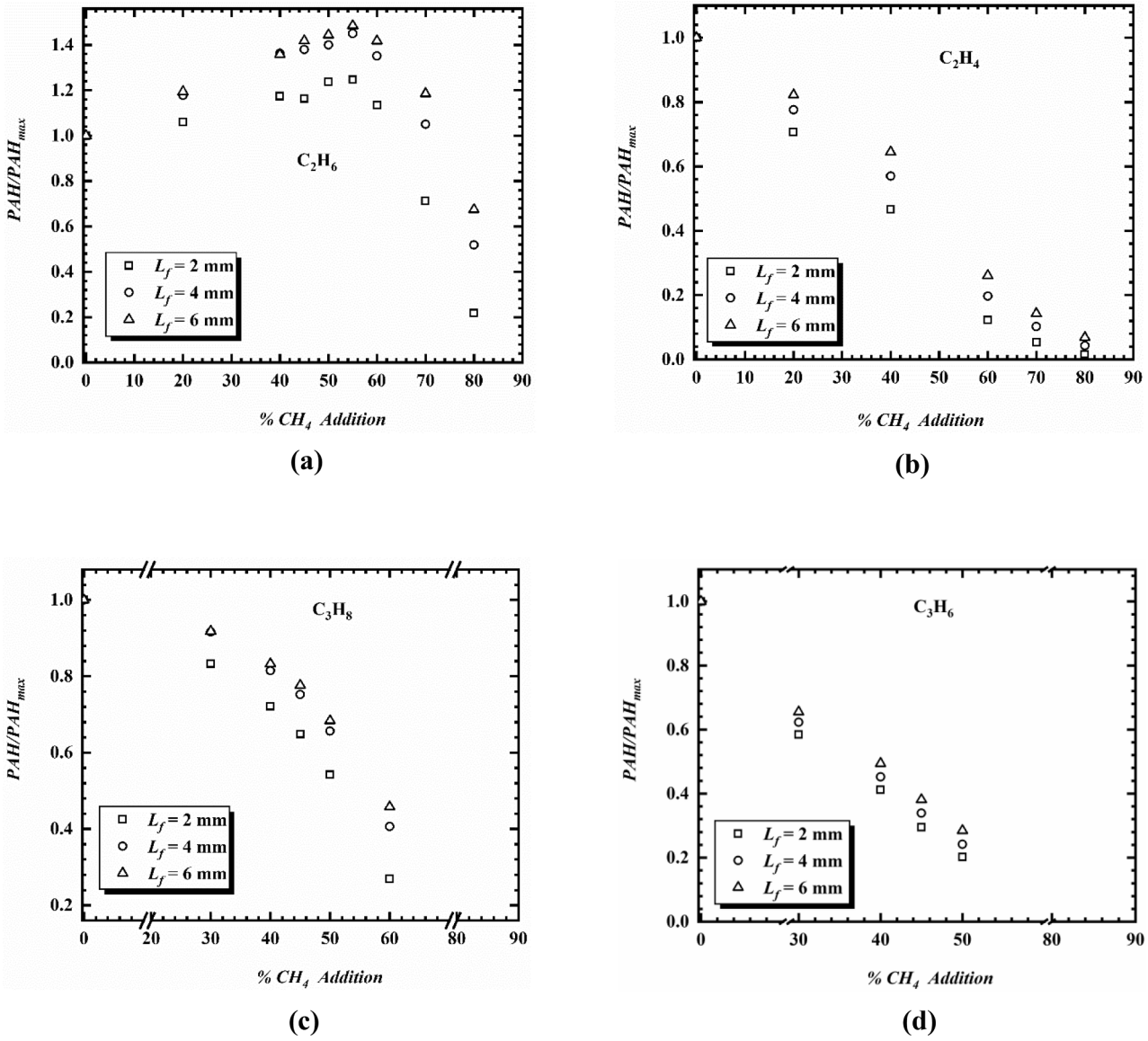

Fig. 6. Variation in the PAH LIF signal normalised using base case value presented as a function of percent CH_4 addition (v/v), at three different HAB for (a) C_2H_6 (b) C_2H_4 (c) C_3H_8 and (d) C_3H_6.

at a rapid rate. Hence, it could be that with the addition of CH_4 in these fuels, the rapid growth of PAHs counteracts the ability of CH_4 to reduce the growth of PAHs (both by mass growth and coagulative mechanism) such that the effect is observed maximally at the point of introduction (closer to the burner lip). Thus, the efficiency of the reaction/growth process in this region closer to the burner lip could potentially make the effect of CH_4 addition more efficient in these positions closer to the burner lip. Also, it can be seen that similar to the observation in the H_2 case, the magnitude of reduction in PAH levels as the L_f increases is relatively the same. Furthermore, comparing PAH reduction between the different hydrocarbon fuels, it can be seen from Fig. 6a – 6d that the trend of reduction in PAH LIF signal with CH_4 addition follows the sequence $C_3H_6 > C_2H_4 > C_3H_8 > C_2H_6$. For example, at a height of 4 mm, with 40% CH_4 addition, there were 55%, 44%, and 18% reduction in PAH LIF signal for C_3H_6, C_2H_4 and C_3H_8 respectively. Similar trends are observed for other heights and percentage CH_4 addition shown in Fig. 6.

Now comparing the effect of H_2 and CH_4 addition on the primary fuels in Fig. 5 and Fig. 6 shows that the addition of CH_4 to C_2H_4 and C_3H_6 showed slightly more variation in PAH LIF signal between heights when compared with H_2 addition to same fuels. Overall reduction in PAH LIF signal was more effective for all fuels with H_2 addition than CH_4 addition. It can be seen that at a height of 2 mm with 30% H_2 addition in Fig. 5, reduction levels in PAH LIF signal were 52%, 60% and 78% for C_3H_6, C_3H_8 and C_2H_4 respectively as against 44%, 28% and 40% for C_3H_6, C_3H_8 and C_2H_4 with 30% CH_4 addition respectively for same conditions in Fig. 6.

To further explain the synergistic effect of the CH_4-C_2H_6 binary mixture, radially integrated PAH LIF signal, PAH (h), for the binary mixture was derived similar to the procedure described in Ref. [44] and is shown in Equation 1 below. The radially integrated PAH LIF signal provides a measure of the total PAH LIF signal in the flame by factoring the change in area of the conically shaped IDF flame.

$$PAH\,(h) = 2\pi \int_0^R rp\,(r,h)\,dr = 2\pi \sum_{i=1}^{R} r_i p\,(r_i,h)\,\Delta r$$

Where r and h represent the radial and axial positions referenced with reference to the burner centreline and the burner exit plane, R is the radius of the integrated path length (~300 mm), the signal at (r,h) is

represented by $p(r,h)$ and Δr is the pixel resolution (~0.25 mm/pixel). Radially integrated PAH LIF signal for binary mixture of C_2H_6 and CH_4 denoted as $PAH_{C_2H_6,m}$ for all CH_4 addition measured was normalised with the maximum value of radially integrated PAH LIF signal of CH_4 base case and plotted against the corresponding fuel component H:C ratio as shown in Fig. 7.

Additionally, normalised values of the corresponding adiabatic temperature (calculated using GASEQ [51]) for the binary mixtures are also presented in Fig. 7. Most reactions leading to PAH and soot formation in combustion systems have been shown to be temperature dependent [28,52]. Hence, determining the temperature of CH_4-C_2H_6 binary fuel mixture could be key to explain the observed trend in PAH formation. Fig. 7 shows that despite the carbon-bound H content increasing (carbon content reducing) from left to right, the PAH LIF steadily increased with CH_4 addition up to a H:C of 3.38 (corresponding to 55% CH_4). Though the PAH LIF decreased beyond this H:C value, the magnitude of PAH LIF was still higher than the value of C_2H_6 base case (represented by H:C of 3.0) up to H:C of 3.54 (corresponding to 70% CH_4). Hence, this increase in PAH levels implies some kind of a synergistic effect between CH_4 and C_2H_6 which has also been observed in literature [18,19,23]. This increase in PAH levels cannot be attributed to increased rates of H_2 abstraction and acetylene addition (HACA), as these reactions are favoured by higher temperature [48], since adiabatic temperatures can be seen in Fig. 7 to decrease monotonically. Hence another possible explanation of the enhancement of PAH levels due to the binary mixture of CH_4 and C_2H_6 has been discussed in the following paragraph.

The role of methyl radicals (CH_3*) in the formation of PAH has been reported previously [19,23,53]. The thermal decomposition of C_2H_6 and CH_4 lead to the production of CH_3* which was shown by Roesler et al. [19] to promote the formation of PAH via the propargyl recombination reaction through the odd-carbon numbered species channel. Even though the addition of CH_4 does increase the H:C ratio of the overall mixture (that is, lowers the carbon content), it is difficult to release the H atom from CH_4, as compared to producing CH_3 radical from C_2H_6. This is because the bond energies of the C–C bond in C_2H_6 (376.1 kJ/mol) is considerably lower than that of the C–H bond in CH_4 (438.6 kJ/mol) [54,55]. Hence, the concentration of CH_3* produced in the binary system possibly outweighs the effect of H-atom released thereby resulting in the enhancement of the formation of PAHs as observed in Fig. 7.

However, it is important to note here that a similar synergistic effect was seen to be absent for the CH_4 and C_3H_8 mixture (see Fig. 6c). Although, the decomposition reactions of C_2H_6 and C_3H_8 produce

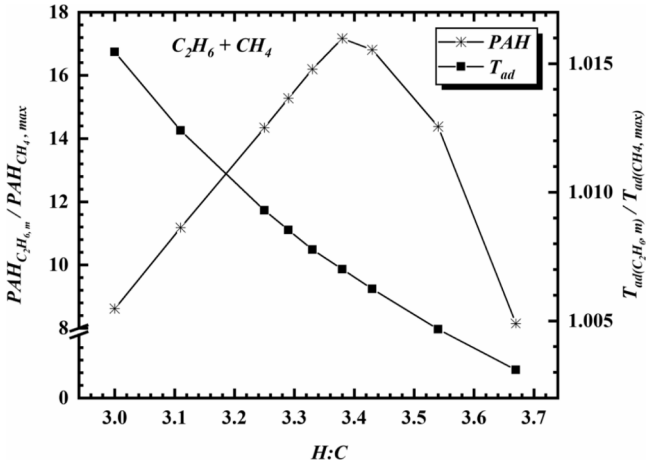

Fig. 7. Radially integrated PAH LIF signal of a mixture of C_2H_6 and CH_4 normalised with the maximum PAH LIF signal of CH_4 and expressed as a function of H:C ratios (same normalisation routine for the mixture adiabatic temperature also presented).

methyl radicals [23], the absence of similar synergistic effect on PAH formation for the CH_4 and C_3H_8 mixture could be attributed to the temperature dependence of PAH formation reaction in the CH_4 and C_3H_8 binary mixture as proposed by Wang *et al.* [56].

3.3. Growth rate of PAH LIF

3.3.1. Effect of H_2 addition

Fig. 8 shows the growth rate of PAH, $d[PAH]/dL_f$ expressed as a function of PAH LIF signal for different levels of H_2 addition in C_2H_6, C_2H_4, C_3H_8, C_3H_6 and CH_4. Following on from the details provided in section 2.4, it is important to reiterate here, that the growth rate refers to the rate of change of PAH LIF signal with L_f. PAH growth rate values as used here were determined relative to distance above the burner lip to indicate PAH formation tendencies as described in section 2.4. Fig. 8 shows that for all the fuels tested, the magnitude of the peak growth rate was highest for the base case (no H_2 addition) and subsequently reduced as the addition of H_2 increased in the primary hydrocarbon fuel. It can also be observed from Fig. 8b and 8c that when the level of addition of H_2 in C_2H_4 and C_3H_8 is above 20% and similarly in Fig. 8e when the H_2 addition in CH_4 is above 10%, the magnitude of the growth rate of PAH becomes similar. This could potentially suggest that there is a point (specific to each fuel) above which the global growth rate of PAH LIF in the fuels tested is not distinguishable even though the local reduction in PAH LIF is still present at this point. It was observed previously in Fig. 5b, 5c, and 5e that, at the same additions of H_2, the local PAH LIF showed significant reduction; with 20% H_2 addition in C_2H_4 and C_3H_8, ~ 60% reduction and 40% reduction in PAH levels were observed respectively while 10% H_2 addition in CH_4 showed ~ 50% reduction in PAH LIF. This trend can be more clearly illustrated with the C_3H_6 case (see Fig. 8d); the curve for the base case (0% H_2) is less steep when compared to the conditions with H_2 addition. It can be seen that as more H_2 is added in C_3H_6, the slope of the respective curves becomes steeper indicating an increase in the potential for growth due to the reduced PAH level. It is expected that prior to observable PAH growth, an activation barrier point at the early growth stage involving typically 1–3 ring PAHs must be exceeded [57]. There is a possibility that because the initial PAH concentration in the C_3H_6 flame with no H_2 addition is orders of magnitude higher than the activation barrier requirements such that further growth in PAH levels as L_f increases is not distinguishable. If this is the case, it is reasonable to assume that there is a possibility that PAH growth in C_3H_6 is self-limiting (slower growth rates). This possibility of self-limiting growth of PAH in the C_3H_6 case suggests that the corresponding slower growth rates could possibly be due to self-assembly of PAHs as an alternative growth mode. Furthermore, from the discussions above, it is evident that the addition of H_2 is not directly proportional to the growth rate of PAH. This is because for all cases studied, even tripling the level of H_2 addition does not result in a corresponding reduction in the rate of growth of PAH.

3.3.2. Effect of CH_4 addition

The rate of growth of PAH for C_2H_6, C_2H_4, C_3H_8, and C_3H_6 with different levels of CH_4 addition is presented in Fig. 9. Similar to the observations in Fig. 8, addition of CH_4 reduces the rate of growth of PAH LIF and above certain CH_4 additions, the growth rate become similar confirming the theory of self-limiting growth characteristics of PAH as discussed previously in the H_2 addition to C_3H_6 case (see section 3.3.1). For example, in C_3H_8 and C_2H_4, between the base case and up to 40% CH_4 addition, the growth rate is not significantly different. With C_2H_4, the growth rate only shows difference with above 60% CH_4 addition levels even though the local concentration of PAH showed marked reduction (~80% reduction in PAH levels in Fig. 6b with 60% CH_4 addition).

Comparing Figs. 8 and 9, it is evident that the addition of CH_4 is not as effective as H_2 in reducing the growth rate of PAH concentration. This could be attributed to difficulty in breaking the C–H bond in CH_4 to

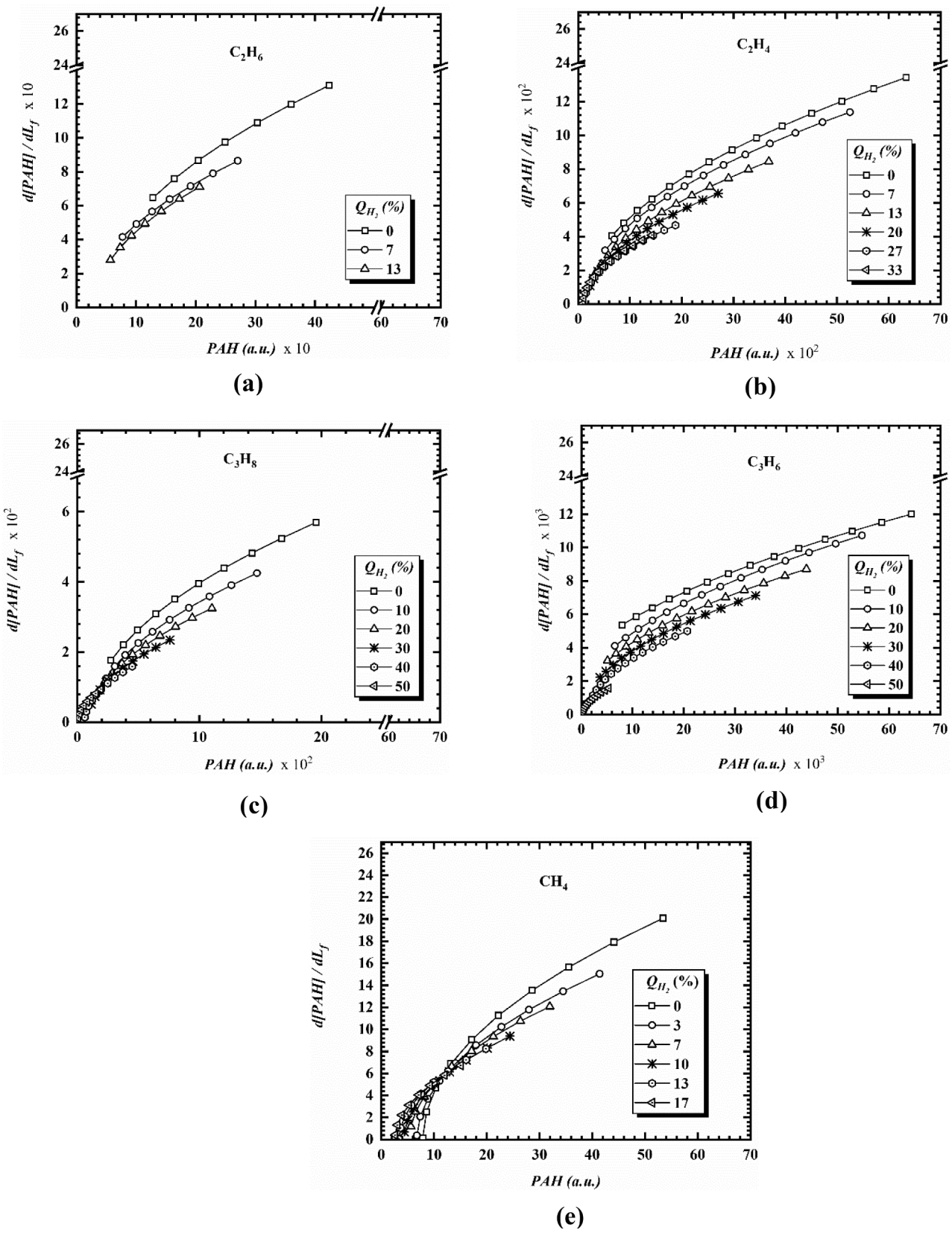

Fig. 8. The growth rate of PAH expressed as a function of PAH LIF signal for different levels of H_2 addition in (a) C_2H_6 (b) C_2H_4 (c) C_3H_8 (d) C_3H_6 and (e) CH_4.

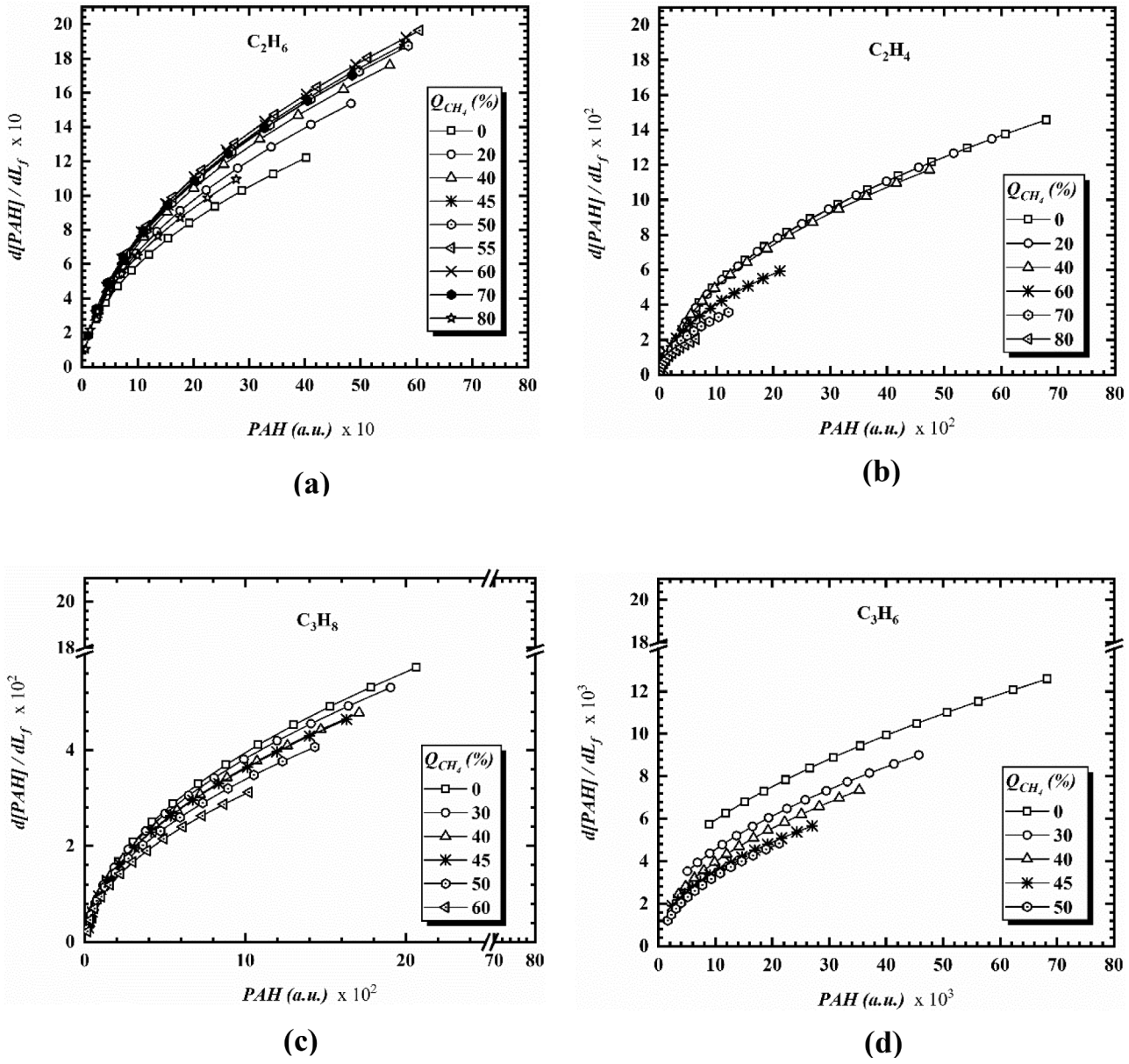

Fig. 9. The growth rate of PAH expressed as a function of PAH LIF signal for different levels of CH_4 addition in (a) C_2H_6 (b) C_2H_4 (c) C_3H_8 and (d) C_3H_6.

release H atom or H_2 as compared to the addition of H_2 which provides H_2 molecule readily available for ring formation and growth of PAHs [23]. Additionally, preferential diffusive effects could play a role in the different effects on PAH growth observed with H_2 and CH_4 addition since H_2 is a considerably more diffusive and reactive molecule than CH_4 (H_2 is about 70% more diffusive than CH_4 [58]).

Now considering the rate of growth of PAH concentration for additions of both H_2 and CH_4, two regions of growth can be observed from Figs. 8 and 9; an initial region where the growth rate of PAH concentration, $d[PAH]/dL_f$ is linear and faster and then a subsequent region where $d[PAH]/dL_f$ becomes non-linear and starts to slow down. The first region corresponds to early formation stages with lower concentration of PAH. This is demonstrated in Figs. 8 and 9 by very steep gradients. This could be attributed to the regions in the flame mainly dominated by active formation of smaller PAHs, and the onset of growth from smaller PAHs to larger PAHs closer to the burner lip. Here, there is an abundance of active sites and higher propensity for further growth (early growth phase). In the experimental study of fuel rich laminar premixed CH_4 flame by Senkan and Castaldi [49], the authors observed that the benzene mole fractions obtained by GC–MS analysis increased rapidly along the reaction zone due to the increase in methyl radicals which enhanced benzene formation through the C_3H_3 recombination routes. A similar rapid increase in the concentration of naphthalene was observed in the main reaction zone of the rich C_2H_4 premixed flame studied by Castaldi et al. [59]. The authors concluded that the increase in the production of benzene coupled with the O_2 molecule available in the main reaction zone favoured the rapid formation of cyclopentadienyl responsible for naphthalene formation. The second region corresponds to regions with increased PAH concentration where possibly only growth to larger PAHs prevails. Here, the concentration of larger PAHs increases until saturation point where the growth slows and possibly nucleation to soot particles commences. A similar saturation was observed by Mitra *et al.* [60] in their study of n-dodecane doped methane co-flow diffusion flame using GC/MS analysis and numerical modelling and observed a plateau in the concentration of cyclopenta(def)phenanthrene (A3R5 – 4 ring PAH) prior to soot nucleation which was attributed to PAHs being incorporated into the young soot. Additionally, from the mole fraction profiles of larger PAHs (3 rings and above)

presented in the experimental studies by Inal and Senkan, [61], the near plateau region can be observed as the HAB increased which was also reproduced by the modelling study in Ref. [17]. It can be seen in Fig. 9a-d that as the concentration of PAH increases, the non-linear growth region dominates showing the saturation clearly. As suggested in the previous sections, this observed saturation in PAH growth could be attributed to the self-limiting growth characteristics of PAH. With increased availability of PAHs for growth and the corresponding reduction in growth rate, it could be argued that the slower growth/self-limiting characteristics is coupled with dynamic self-assembly of PAHs (maybe through dimerisation). Considering the addition of H_2 and CH_4, it can be observed that the addition of both fuels tends to move the trend to the former region (that is the region of linear growth rate with steeper gradients) with H_2 showing more effectiveness. Also, the rate of growth of PAH concentration have been shown to reduce with increasing volume of the secondary fuel (H_2 or CH_4) in the binary mixture.

To further explain the relationship between PAH LIF signal and the PAH growth rate for all the conditions studied, the PAH LIF signal and their corresponding growth rate for all the cases in Figs. 8 and 9 are presented as a log–log plot in Fig. 10. Fig. 10 also shows all binary fuel mixtures investigated grouped into various range of H:C ratios. The growth rate function, $d[PAH]/dL_f$ is denoted by GR_{PAH}. The data shown in this figure include the H:C ratios of all the mixtures that have been achieved by the addition of either H_2 (non-carbon-bound H represented by subscript m) or CH_4 (carbon-bound H represented by subscript f). A linear regression line has been fitted through the data in Fig. 10 to quantify (albeit, within margins of error) the effect of the addition of these secondary fuels on the growth rate of PAH in the primary fuels studied. Consequently, the relationship between the growth rate and the PAH LIF signal for the mixtures investigated follows the empirical correlation:

$$ln\,[GR_{PAH}] = 0.8609 * ln\,[PAH] + ln\,[1.1383].$$

which could be further simplified to:

$$GR_{PAH} = 1.1383 * PAH^{0.8609}.$$

This empirical equation can be used to determine PAH growth rate for other hydrocarbon fuels/fuel mixtures with H:C ratios similar to those investigated in this study.

The following paragraphs provide some further insights from Fig. 10 and the empirical correlation. The early stages of PAH formation and growth is expected to be dominated by the reactions involving smaller PAHs. It is expected that at this stage (typically lower in the flame closer to the burner exit nozzle), the rate of reaction is fast (and possibly efficient) which implies that the effect of the added H_2 could be very effective leading to lower concentration of PAH. This is in agreement with the observation by Guo *et al.* [10] in their numerical study of soot formation in H_2 and C_2H_4/air diffusion flame. The authors reported lower concentrations of 4-ring PAHs at lower heights in the flame as compared to the corresponding higher concentration at higher heights with the addition of H_2. However, beyond this region of low concentration (that is, the lower end of the graph), a linear correlation (as mentioned earlier) can be seen in Fig. 10. Notably, the gradient of the log of the growth rate lies within a band irrespective of the fuel bonding, molecular structure and the H:C ratio of the fuel mixtures. This implies that though there exist significant difference on the effects the addition of either H_2 (non-carbon-bound H) or CH_4 (carbon-bound H) has on the growth of PAHs as discussed in previous sections (see Figs. 5 and 6), there is a limit to how much the PAH grows as PAH LIF signal increases irrespective of the starting point or primary fuel.

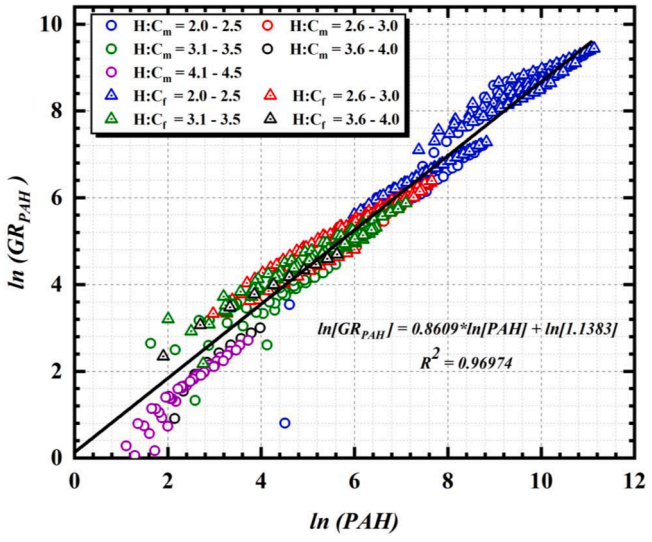

Fig. 10. Rate of growth of PAH for all fuels according to different H:C ratio for the carbon-bound H represented by subscript f, and non-carbon-bound H represented by subscript m and linear regression fit through the data showing the band region of the growth rate.

To reiterate, in Fig. 10, the fuel mixtures with higher H:C ratio range corresponds to lower PAH concentration and growth rate. As expected, fuels/fuel mixtures which have higher H:C ratio (lower carbon content) produce less PAHs and hence occupy the lower end of the log–log plot.

Additionally, it can be seen from Fig. 10 that the starting point for each H:C range (representative of the fuel/mixture molecular structure) is different; this is expected as PAH formation and increase in concentration will always be dependent on the molecular structure of the hydrocarbon fuel at the onset of PAH formation. For example, initially PAH formation (and concentration) from a hydrocarbon fuel with lower H:C ratio (high carbon content) such as C_3H_6 (unsaturated hydrocarbon) would be greater when compared with a hydrocarbon fuel of higher H:C ratio such as CH_4 (saturated hydrocarbon) (see Figs. 8 and 9). However, this effect seems to become insignificant on the growth rate function as the concentration of PAH and time (in terms of L_f) increases. A similar observation was made by Keller *et al.* [62] which confirmed that PAHs undergo additional reactions simultaneously with growth reactions in the oxidation zone of flames to rapidly form same products independent of the starting fuel. Fig. 10 shows that even though the different H:C range start from different points on the curve, the slope is the same except at the higher H:C ratio values of 4.1–4.5. However, the gradient of the mixtures with H:C ratios between 4.1 and 4.5 by extrapolation achieves same slope when *ln [PAH]* value grows to around 6.5. This could potentially suggest that the growth rate of PAH is primarily dependent on the starting fuel at the early stages of PAH formation, beyond which the level of dependence follows a log–log linear relationship with the empirical expression: $GR_{PAH} = 1.1383 * PAH^{0.8609}$.

4. Conclusions

This paper presented an experimental study of PAH formation and growth characteristics in various binary fuel mixtures in a laminar inverse diffusion flame configuration using simultaneous OH-PAH planar laser induced fluorescence (PLIF). OH-PLIF was used to represent peak temperature regions in the flame front. The adiabatic flame temperatures of the binary fuel mixtures were calculated using GASEQ. First, H_2 was added to CH_4, C_2H_6, C_3H_8, C_2H_4 and C_3H_6 and thereafter, CH_4 was added to C_2H_6, C_3H_8, C_2H_4 and C_3H_6 respectively. It was shown that the addition of H_2 and CH_4 to hydrocarbon flames reduced the growth rate of PAH. However, the level of reduction to the growth rate of PAH was still found to be dependent on the local PAH concentration that could be linked to sooting tendency of the fuel. Other conclusions for this study are summarised below:

- It was found that the addition of H_2 to C_2H_4, C_3H_8 and C_3H_6 showed no significant variation in the magnitude of PAH reduction as the height along the flame front, L_f increases. However, with the addition of H_2 to CH_4, higher reduction in PAH levels was observed at higher L_f due to the effectiveness of H_2 in impeding the growth of smaller

PAHs closer to the burner lip, hence resulting in reduced growth to larger PAHs. However, the addition of CH_4 showed higher reductions at lower L_f for all the fuels tested. H_2 addition was observed to be more effective than CH_4 in reducing PAH LIF signal.

- The IDF binary mixture of CH_4 and C_2H_6 showed a distinctive synergistic effect on PAH concentration for up to 70% of CH_4 addition even though the H:C ratio increased (which implies a corresponding reduction in carbon content). This was potentially attributed to the formation of CH_3* radicals which may promote PAH formation via the propargyl recombination route.
- The addition of both H_2 and CH_4 reduced the rate of growth of PAH concentration with H_2 showing higher reductions. The addition of both fuels shows two distinct regions; a steep growth region (linear) followed by a slower growth region (non-linear).
- Though there exists significant difference between the addition of H_2 (non-carbon-bound H) and CH_4 (carbon-bound H) on the growth rate of PAHs, there is a limit to how much the PAH grows irrespective of the starting fuel.
- The growth rate of PAH was observed to be primarily dependent on the starting fuel (that is, dependent on the H:C ratio) at the early stages of PAH formation, beyond which the level of dependence follows a log–log linear relationship with the empirical expression: $GR_{PAH} = 1.1383^{*}\ PAH^{0.8609}$.

Declaration of Competing Interest

The authors declare that they have no known competing financial interests or personal relationships that could have appeared to influence the work reported in this paper.

Acknowledgements

The authors would like to acknowledge UKRI Future Leaders Fellowship (MR/T019735/1), EPSRC (EP/P003036/1) and the Nigerian Petroleum Technology Development Fund (PTDF) (PTDF/ED/PHD/ECE/97/16) for their financial support towards this work.

References

[1] Kennedy IM. The health effects of combustion-generated aerosols. Proc Combust Inst 2007;31 II:2757–70. 10.1016/j.proci.2006.08.116.
[2] Michelsen HA. Probing soot formation, chemical and physical evolution, and oxidation: A review of in situ diagnostic techniques and needs. Proc Combust Inst 2017;36:717–35. https://doi.org/10.1016/j.proci.2016.08.027.
[3] Bond TC, Doherty SJ, Fahey DW, Forster PM, Berntsen T, Deangelo BJ, et al. Bounding the role of black carbon in the climate system: A scientific assessment. J Geophys Res Atmos 2013;118:5380–552. https://doi.org/10.1002/jgrd.50171.
[4] Richter H, Howard J. Formation of polycyclic aromatic hydrocarbons and their growth to soot - a review of chemical reaction pathways. Prog Energy Combust Sci 2000;26:565–608. https://doi.org/10.1016/S0360-1285(00)00009-5.
[5] A D'Anna, A D'Alessio PM. Soot Formation in Combustion—Mechanisms and Models. 1st ed. Berlin: Springer-Verlag; 1994. 10.1007/978-3-642-85167-4_10.
[6] Skjøth-Rasmussen MS, Glarborg P, Østberg M, Johannessen JT, Livbjerg H, Jensen AD, et al. Formation of polycyclic aromatic hydrocarbons and soot in fuel-rich oxidation of methane in a laminar flow reactor. Combust Flame 2004;136:91–128. https://doi.org/10.1016/j.combustflame.2003.09.011.
[7] Zhang Y, Wang L, Liu P, Guan B, Ni H, Huang Z, et al. Experimental and kinetic study of the effects of CO2and H2O addition on PAH formation in laminar premixed C2H4/O2/Ar flames. Combust Flame 2018;192:439–51. https://doi.org/10.1016/j.combustflame.2018.01.050.
[8] McEnally CS, Pfefferle LD. The effect of nitrogen dilution on nonfuel hydrocarbons in laminar nonpremixed flames. Combust Sci Technol 2000;151:133–55. https://doi.org/10.1080/00102200008924217.
[9] Wang Y, Liu X, Gu M, An X. Numerical Simulation of the Effects of Hydrogen Addition to Fuel on the Structure and Soot Formation of a Laminar Axisymmetric Coflow C2H4/(O2-CO2) Diffusion Flame. Combust Sci Technol 2019;191:1743–68. https://doi.org/10.1080/00102202.2018.1532413.
[10] Guo H, Liu F, Smallwood GJ, Gülder ÖL. Numerical study on the influence of hydrogen addition on soot formation in a laminar ethylene-air diffusion flame. Combust Flame 2006;145:324–38. https://doi.org/10.1016/j.combustflame.2005.10.016.
[11] Liu F, Ai Y, Kong W. Effect of hydrogen and helium addition to fuel on soot formation in an axisymmetric coflow laminar methane/air diffusion flame. Int J Hydrogen Energy 2014;39:3936–46. https://doi.org/10.1016/j.ijhydene.2013.12.151.
[12] Du DX, Axelbaum RL, Law CK. Soot formation in strained diffusion flames with gaseous additives. Combust Flame 1995;102:11–20. https://doi.org/10.1016/0010-2180(95)00043-6.
[13] Do H-Q, Faccinetto A, Tran L-S, Desgroux P, Gasnot L, El Bakali A, et al. Hydrogen as a fuel additive in laminar premixed methane flames: Impact on the nucleation and growth of soot particles. Fuel 2022;315:123125. https://doi.org/10.1016/j.fuel.2021.123125.
[14] Sarathy SM, Kukkadapu G, Mehl M, Wang W, Javed T, Park S, et al. Ignition of alkane-rich FACE gasoline fuels and their surrogate mixtures. Proc Combust Inst 2015;35:249–57. https://doi.org/10.1016/j.proci.2014.05.122.
[15] Zhang C, Chen L, Ding S, Xu H, Li G, Consalvi J-L, et al. Effects of soot inception and condensation PAH species and fuel preheating on soot formation modeling in laminar coflow CH4/air diffusion flames doped with n-heptane/toluene mixtures. Fuel 2019;253:1371–7. https://doi.org/10.1016/j.fuel.2019.05.100.
[16] Wang Y, Chung SH. Soot formation in laminar counterflow flames. Prog Energy Combust Sci 2019;74:152–238. https://doi.org/10.1016/j.pecs.2019.05.003.
[17] Park S, Wang Y, Chung SH, Sarathy SM. Compositional effects on PAH and soot formation in counterflow diffusion flames of gasoline surrogate fuels. Combust Flame 2017;178:46–60. https://doi.org/10.1016/j.combustflame.2017.01.001.
[18] Trottier S, Guo H, Smallwood GJ, Johnson MR. Measurement and modeling of the sooting propensity of binary fuel mixtures. Proc Combust Inst 2007;31 I:611–9. 10.1016/j.proci.2006.07.229.
[19] Roesler JF, Martinot S, McEnally CS, Pfefferle LD, Delfau JL, Vovelle C. Investigating the role of methane on the growth of aromatic hydrocarbons and soot in fundamental combustion processes. Combust Flame 2003;134:249–60. https://doi.org/10.1016/S0010-2180(03)00093-2.
[20] Yan F, Xu L, Wang Y, Park S, Sarathy SM, Chung SH. On the opposing effects of methanol and ethanol addition on PAH and soot formation in ethylene counterflow diffusion flames. Combust Flame 2019;202:228–42. https://doi.org/10.1016/j.combustflame.2019.01.020.
[21] Wang Y, Park S, Sarathy SM, Chung SH. A comparative study on the sooting tendencies of various 1-alkene fuels in counterflow diffusion flames. Combust Flame 2018;192:71–85. https://doi.org/10.1016/j.combustflame.2018.01.033.
[22] Hwang JY, Chung SH, Lee W. Effects of oxygen and propane addition on soot formation in counterflow ethylene flames and the role of C3 chemistry. Symp Combust 1998;27:1531–8. https://doi.org/10.1016/S0082-0784(98)80561-4.
[23] Yoon SS, Lee SM, Chung SH. Effect of mixing methane, ethane, propane, and propene on the synergistic effect of PAH and soot formation in ethylene-base counterflow diffusion flames. Proc Combust Inst 2005;30:1417–24. https://doi.org/10.1016/j.proci.2004.08.038.
[24] Yoon SS, Anh DH, Chung SH. Synergistic effect of mixing dimethyl ether with methane, ethane, propane, and ethylene fuels on polycyclic aromatic hydrocarbon and soot formation. Combust Flame 2008;154:368–77. https://doi.org/10.1016/J.COMBUSTFLAME.2008.04.019.
[25] Liu F, He X, Ma X, Zhang Q, Thomson MJ, Guo H, et al. An experimental and numerical study of the effects of dimethyl ether addition to fuel on polycyclic aromatic hydrocarbon and soot formation in laminar coflow ethylene/air diffusion flames. Combust Flame 2011;158:547–63. https://doi.org/10.1016/j.combustflame.2010.10.005.
[26] Shaddix CR, Williams TC. Measurements of the velocity field in laminar ethylene inverse jet diffusion flames. Combust Flame 2009;156:942–5. https://doi.org/10.1016/j.combustflame.2009.01.017.
[27] Liu F, Hua Y, Wu H, Lee CFF, Li Y. Experimental investigation of polycyclic aromatic hydrocarbons growth characteristics of gasoline mixed with methanol, ethanol, or n-butanol in laminar diffusion flames. Energy Fuels 2018;32:6823–33. https://doi.org/10.1021/acs.energyfuels.8b00693.
[28] Sidebotham GW, Glassman I. Flame temperature, fuel structure, and fuel concentration effects on soot formation in inverse diffusion flames. Combust Flame 1992;90:269–83. https://doi.org/10.1016/0010-2180(92)90088-7.
[29] Santamaría A, Mondragón F, Molina A, Marsh ND, Eddings EG, Sarofim AF. FT-IR and1H NMR characterization of the products of an ethylene inverse diffusion flame. Combust Flame 2006;146:52–62. https://doi.org/10.1016/j.combustflame.2006.04.008.
[30] Blevins LG, Fletcher RA, Benner BA, Steel EB, Mulholland GW. The existence of young soot in the exhaust of inverse diffusion flames. Proc Combust Inst 2002;29:2325–33. https://doi.org/10.1016/S1540-7489(02)80283-8.
[31] Dobbins RA. Hydrocarbon nanoparticles formed in flames and diesel engines. Aerosol Sci Technol 2007;41:485–96. https://doi.org/10.1080/02786820701225820.
[32] Mikofski MA, Williams TC, Shaddix CR, Blevins LG. Flame height measurement of laminar inverse diffusion flames. Combust Flame 2006;146:63–72. https://doi.org/10.1016/j.combustflame.2006.04.006.
[33] Zizak G, Cignoli F, Montas G, Beneccchi S, Dondè R. Detection of aromatic hydrocabons in the exhaust gases of a i.c. engine by laser-induced fluorescence technique. Recent Res Devel Appl Spectro 1996;1.
[34] Singh P, Sung CJ. PAH formation in counterflow non-premixed flames of butane and butanol isomers. Combust Flame 2016;170:91–110. https://doi.org/10.1016/j.combustflame.2016.05.009.
[35] Lee SM, Yoon SS, Chung SH. Synergistic effect on soot formation in counterflow diffusion flames of ethylene-propane mixtures with benzene addition. Combust Flame 2004;136:493–500. https://doi.org/10.1016/j.combustflame.2003.12.005.
[36] Xiao J, Austin E, Roberts WL. Relative polycyclic aromatic hydrocarbon concentrations in unsteady counterflow diffusion flames. Combust Sci Technol 2005;177:691–713. https://doi.org/10.1080/00102200590917239.

[37] Vander Wal RL. LIF-LII measurements in a turbulent gas-jet flame. Exp Fluids 1997; 23:281–7. https://doi.org/10.1007/s003480050112.
[38] Beretta F, Cincotti V, D'Alessio A, Menna P. Ultraviolet and visible fluorescence in the fuel pyrolysis regions of gaseous diffusion flames. Combust Flame 1985;61: 211–8. https://doi.org/10.1016/0010-2180(85)90102-6.
[39] Wu J, Song KH, Litzinger T, Lee SY, Santoro R, Linevsky M. Reduction of PAH and soot in premixed ethylene-air flames by addition of dimethyl ether. Combust Sci Technol 2006;178:837–63. https://doi.org/10.1080/00102200500269942.
[40] Ezenwajiaku TM, Doan NAK, Swaminathan N, Balachandran R. Study of polycyclic aromatic hydrocarbons (PAHs) in hydrogen-enriched methane diffusion flames. Int J Hydrogen Energy 2019;44:7642–55. https://doi.org/10.1016/j.ijhydene.2019.01.253.
[41] Frenklach M. Reaction mechanism of soot formation in flames. Phys Chem Chem Phys 2002;4:2028–37. https://doi.org/10.1039/b110045a.
[42] Faccinetto A, Irimiea C, Minutolo P, Commodo M, D'Anna A, Nuns N, et al. Evidence on the formation of dimers of polycyclic aromatic hydrocarbons in a laminar diffusion flame. Commun Chem 2020;3:1–8. https://doi.org/10.1038/s42004-020-00357-2.
[43] Mercier X, Carrivain O, Irimiea C, Faccinetto A, Therssen E. Dimers of polycyclic aromatic hydrocarbons: The missing pieces in the soot formation process. Phys Chem Chem Phys 2019;21:8285–94. https://doi.org/10.1039/c9cp00394k.
[44] Mikofski MA, Williams TC, Shaddix CR, Fernandez-Pello AC, Blevins LG. Structure of laminar sooting inverse diffusion flames. Combust Flame 2007;149:463–78. https://doi.org/10.1016/J.COMBUSTFLAME.2007.01.006.
[45] Wang H, Frenklach M. A detailed kinetic modeling study of aromatics formation in laminar premixed acetylene and ethylene flames. Combust Flame 1997;110: 173–221. https://doi.org/10.1016/S0010-2180(97)00068-0.
[46] Frenklach M. On the driving force of PAH production. Symp Combust 1988;22: 1075–82.
[47] Gülder ÖL, Snelling DR, Sawchuk RA. Influence of hydrogen addition to fuel on temperature field and soot formation in diffusion flames. Symp Combust 1996;26: 2351–8. https://doi.org/10.1016/S0082-0784(96)80064-6.
[48] Hwang JY, Lee W, Kang HG, Chung SH. Synergistic effect of ethylene-propane mixture on soot formation in laminar diffusion flames. Combust Flame 1998;114: 370–80. https://doi.org/10.1016/S0010-2180(97)00295-2.
[49] Senkan S, Castaldi M. Formation of polycyclic aromatic hydrocarbons (PAH) in methane combustion: Comparative new results from premixed flames. Combust Flame 1996;107:141–50. https://doi.org/10.1016/0010-2180(96)00044-2.
[50] Hepp H, Siegmann K, Sattler K. New aspects of growth mechanisms for polycyclic aromatic hydrocarbons in diffusion flames. Chem Phys Lett 1995;233:16–22. https://doi.org/10.1016/0009-2614(94)01433-V.
[51] Morley C. GASEQ, A Chemical Windows, Equilibrium Program for 0.79. 2005.
[52] Appel J, Bockhorn H, Frenklach M. Kinetic modeling of soot formation with detailed chemistry and physics: laminar premixed flames of C2 hydrocarbons. Combust Flame 2000;121:122–36. https://doi.org/10.1016/S0010-2180(99)00135-2.
[53] Bittner JD, Howard JB. Composition profiles and reaction mechanisms in a near-sooting premixed benzene/oxygen/argon flame. Symp Combust 1981;18:1105–16. https://doi.org/10.1016/S0082-0784(81)80115-4.
[54] Solomons TWG, Fryhle CB. Organic Chemistry. Tenth edit. New York: Wiley; 2011.
[55] Ruscic B. Active Thermochemical Tables: Sequential Bond Dissociation Enthalpies of Methane, Ethane, and Methanol and the Related Thermochemistry. J Phys Chem A 2015;119:7810–37. https://doi.org/10.1021/acs.jpca.5b01346.
[56] Wang W, Xu L, Yan J, Wang Y. Temperature dependence of the fuel mixing effect on soot precursor formation in ethylene-based diffusion flames. Fuel 2020;267. https://doi.org/10.1016/j.fuel.2020.117121.
[57] Zhang T, Mu G, Zhang S, Hou J. Formation pathways of polycyclic aromatic hydrocarbons (PAHs) in butane or butadiene flames. RSC Adv 2021;11:5629–42. https://doi.org/10.1039/d0ra08744k.
[58] Zhao X, Jin H. Correlation for self-diffusion coefficients of H2, CH4, CO, O2 and CO2 in supercritical water from molecular dynamics simulation. Appl Therm Eng 2020;171. https://doi.org/10.1016/j.applthermaleng.2020.114941.
[59] Castaldi MJ, Marinov NM, Melius CF, Huang J, Senkan SM. Experimental and modeling investigation of aromatic and polycyclic aromatic hydrocarbon formation in a premixed ethylene flame. Symp Combust 1996;26:693–702.
[60] Mitra T, Zhang T, Sediako AD, Thomson MJ. Understanding the formation and growth of polycyclic aromatic hydrocarbons (PAHs) and young soot from n-dodecane in a sooting laminar coflow diffusion flame. Combust Flame 2019;202: 33–42. https://doi.org/10.1016/j.combustflame.2018.12.010.
[61] Inal F, Senkan SM. Effects of equivalence ratio on species and soot concentrations in premixed n-heptane flames. Combust Flame 2002;131:16–28. https://doi.org/10.1016/S0010-2180(02)00388-7.
[62] Keller A, Kovacs R, Homann K-H. Large molecules, ions, radicals, and small soot particles in fuel-rich hydrocarbon flames; Part IV: Positive ions of polycyclic aromatic hydrocarbons (PAH) in low-pressure premixed flames of benzene and oxygen. Phys Chem Chem Phys 2000;2:1667–75. https://doi.org/10.1016/S0010-2180(00)00225-X.